Homogenization induced by chaotic mixing and diffusion in an oscillatory chemical reaction

I. Z. Kiss,[1,*] J. H. Merkin,[2] and Z. Neufeld[3]
[1]*Department of Zoology, University of Oxford, South Parks Road, Oxford, OX1 3PS, United Kingdom*
[2]*Department of Applied Mathematics, University of Leeds, Leeds, LS2 9JT, United Kingdom*
[3]*Center for Nonlinear Studies, Los Alamos National Laboratory, Los Alamos, New Mexico 87545, USA*
(Received 28 February 2004; published 30 August 2004)

A model for an imperfectly mixed batch reactor with the chlorine dioxide-iodine-malonic acid (CDIMA) reaction, with the mixing being modelled by chaotic advection, is considered. The reactor is assumed to be operating in oscillatory mode and the way in which an initial spatial perturbation becomes homogenized is examined. When the kinetics are such that the only stable homogeneous state is oscillatory then the perturbation is always entrained into these oscillations. The rate at which this occurs is relatively insensitive to the chemical effects, measured by the Damköhler number, and is comparable to the rate of homogenization of a passive contaminant. When both steady and oscillatory states are stable, spatially homogeneous states, two possibilities can occur. For the smaller Damköhler numbers, a localized perturbation at the steady state is homogenized within the background oscillations. For larger Damköhler numbers, regions of both oscillatory and steady behavior can co-exist for relatively long times before the system collapses to having the steady state everywhere. An interpretation of this behavior is provided by the one-dimensional Lagrangian filament model, which is analyzed in detail.

DOI: 10.1103/PhysRevE.70.026216 PACS number(s): 82.40.Bj, 82.40.Ck

I. INTRODUCTION

It is well known that mixing can be greatly enhanced by the chaotic motion of fluid elements in unsteady laminar flows [1–3]. An initially smooth distribution of a passive contaminant (passive scalar) is distorted by the chaotic advection and develops a complex spatial structure with high concentration gradients, enhancing diffusive transport. This can then lead to the decay of the concentration fluctuations and homogenization [4–6]. An imperfectly mixed environment is a common characteristic of many real chemical and biological processes. Even very small fluctuations in temperature or concentration in the medium, presumed to be totally homogeneous, can have important effects in the presence of nonlinear dynamics. In laboratory experiments, for example, strong stirring is frequently used to achieve good homogeneity of the reactants. Nevertheless, perfect homogeneity can never be fully realized and it has been observed that experimental measurements can depend on stirring rates [7–10].

The aim of this paper is to study the evolution of initial inhomogeneities in a system driven by nonlinear chemical dynamics corresponding to an oscillatory chemical reaction coupled with diffusion and chaotic advection. In the absence of transport processes (chaotic mixing and diffusion) the chemical dynamics at each point in the domain of interest can be regarded as an independent nonlinear oscillator. Nonuniform initial conditions would thus result in a set of identical oscillators, each oscillating with different phases. Therefore we can regard homogenization due to the combined effects of advection and diffusion as a synchronization of these local oscillators.

*Corresponding author. Fax: +44-1865-310-447; email address: istvan.kiss@zoo.ox.ac.uk

The specific chemical reaction that we consider is the chlorine dioxide-iodine-malonic acid (CDIMA) reaction, which has been shown to exhibit oscillatory behavior both experimentally [11,12] and in the kinetics derived to describe the reaction [13,14]. One feature of this model is that the oscillations can arise through a subcritical Hopf bifurcation, giving the possibility of multistability, by the coexistence of a stable steady state and a stable limit cycle in a certain range of the parameters. For the flow we take an oscillatory shear flow [15]. The exact nature of the flow is not especially important, all we really require is that the time-dependent flow can generate chaotic advection of fluid elements, i.e., it is chaotic when viewed in its Lagrangian description. The oscillating shear flow has this property, our choice being motivated by ease of implementation for the numerical simulations. The basic situation we address is that of a system initially oscillating homogeneously in space with some initial spatial perturbation applied. The main question is whether the system returns to spatially homogeneous oscillations or not, and, if it does, how is this achieved? Does the mixing process have any significant effect on the chemical reaction beyond what would be seen for a passive contaminant? Alternatively, the problem can be thought of as how a continuum distribution of identical oscillators coupled by diffusion and chaotic advection will respond to an initial difference in phase.

We start by describing our model and deriving the corresponding advection-reaction-diffusion equations. A numerical study of these two-dimensional equations is then undertaken, considering separately the cases when the Hopf bifurcation in the kinetic system is supercritical and when it is subcritical. In the first case the system is taken to be oscillating homogeneously in space before a perturbation is applied. In the second case when the system has two stable states (homogeneous steady state and stable limit cycle) two different scenarios are investigated: (i) the system is in the

oscillatory state everywhere except in a small region which is set to the steady state, and (ii) most of the system is in the steady state and is oscillating in a small part of the domain. In both cases the dependence of the final state of the system on the relative strengths of the stirring rate and rate of the chemical reaction is investigated.

A one-dimensional Lagrangian model has previously proved to be useful in giving insight into the behavior of two-dimensional (2D) advection-reaction-diffusion problems [16–20] (for earlier work see Refs. [21–26]). This one-dimensional model is analyzed in detail and provides an interpretation of some of the behavior seen in the full model.

II. MODEL

The general problem can be described by a set of N advection-diffusion-reaction equations, corresponding to a stirred batch reactor,

$$\frac{\partial c_i}{\partial t} + \mathbf{v}(\mathbf{r},t) \cdot \nabla c_i = F_i(c_1, \ldots, c_N) + D_i \nabla^2 c_i, \tag{1}$$

where $\mathbf{v}(\mathbf{r},t)$ is an incompressible time-dependent spatially smooth flow advecting fluid elements chaotically within a finite domain. The flow is presumed to be independent of the chemical concentrations. The set of functions F_i models the chemical interactions between different components chosen such that, in the case of spatially uniform concentrations, the reaction dynamics

$$\dot{c}_i = F_i(c_1, \ldots, c_N) \quad (i = 1, \ldots, N) \tag{2}$$

has a stable limit cycle of period T_c, i.e.,

$$c_i(t + T_c) = c_i(t) \ (i = 1, \ldots, N) \quad \text{for all } t. \tag{3}$$

Chaotic mixing is modelled by a simple time-periodic velocity field describing a closed flow within a finite domain (a periodic shear flow). We note that our results are expected to remain valid for a wide range of two-dimensional laminar flows capable of producing repeated stretching and folding of fluid elements, a common characteristic of any chaotic advection. The velocity field, $\mathbf{v}=(v_x,v_y)$,

$$v_x(x,y,t) = \begin{cases} \dfrac{AL}{T_f}\sin(2\pi y + \phi_i), & \text{if } t \in \left[nT_f, n+\dfrac{1}{2}T_f \right) \\ 0, & \text{if } t \in \left[n+\dfrac{1}{2}T_f, (n+1)T_f \right), \end{cases} \tag{4}$$

$$v_y(x,y,t) = \begin{cases} 0, & \text{if } t \in \left[nT_f, n+\dfrac{1}{2}T_f \right) \\ \dfrac{AL}{T_f}\sin(2\pi x + \phi_{i+1}), & \text{if } t \in \left[n+\dfrac{1}{2}T_f, (n+1)T_f \right), \end{cases} \tag{5}$$

is defined on a doubly periodic square domain of length L. T_f is the period and A is a parameter (we use $A=1.4$), that controls the chaotic behavior of the flow. The Lyapunov exponent of this flow has the same order of magnitude as $1/T_f$. Transport barriers due to Kolmogorov-Arnold-Moser (KAM) tori, typically present in periodically driven conservative systems, can be avoided by breaking the periodicity using a random phase ϕ_i, different in each half of the time period.

The oscillating nonlinear chemical dynamics that we use is the chlorine dioxide-iodine-malonic acid (CDIMA) reaction, following the Lengyel-Epstein kinetic scheme [11,14]. In this reaction, the reactor is supplied with malonic acid (MA), chlorine dioxide (ClO_2), and iodine (I_2). The important intermediate species are iodide I^- and chlorite ClO_2^- ions, which participate in the following three component stoichiometric processes:

$$\mathrm{MA} + \mathrm{I_2} \rightarrow \mathrm{IMA} + \mathrm{I^-} + \mathrm{H^+}, \quad r_1 = \frac{k_{1\alpha}[\mathrm{MA}][\mathrm{I_2}]}{k_{1\beta} + [\mathrm{I_2}]}, \tag{6}$$

$$\mathrm{ClO_2} + \mathrm{I^-} \rightarrow \mathrm{ClO_2^-} + \frac{1}{2}\mathrm{I_2}, \quad r_2 = k_2[\mathrm{ClO_2}][\mathrm{I^-}], \tag{7}$$

$$\mathrm{ClO_2^-} + 4\mathrm{I^-} + 4\mathrm{H^+} \rightarrow \mathrm{Cl^-} + 2\mathrm{I_2} + 2\mathrm{H_2O},$$

$$r_3 = \frac{k_{3\beta}[\mathrm{ClO_2^-}][\mathrm{I_2}][\mathrm{I^-}]}{k_{3\gamma} + [\mathrm{I^-}]^2}. \tag{8}$$

The concentrations of the "pool chemicals" MA, ClO_2, and I_2 are experimentally variable parameters and the products IMA and Cl^- are not considered explicitly. c_1 and c_2 denote the concentrations of I^- and ClO_2^-, respectively. The chemical system can be described by the two-variable model that evolves according to

$$\dot{c}_1 = r_1 - r_2 - 4r_3, \tag{9}$$

$$\dot{c}_2 = r_2 - r_3. \tag{10}$$

After substituting the velocity field (4) and (5), and the nonlinear chemical dynamics (9) and (10) into the original advection-diffusion-reaction (1), we introduce the following transformation to obtain dimensionless variables:

$$\overline{c}_1 = \frac{c_1}{U_s}, \quad \overline{c}_2 = \frac{c_2}{V_s}, \quad \overline{t} = \frac{tU_0}{L}, \quad \overline{\mathbf{r}} = \frac{\mathbf{r}}{L}, \quad \overline{\mathbf{v}} = \frac{\mathbf{v}}{U_0}, \tag{11}$$

where L and $U_0=L/T_f$ are the characteristic length and velocity scales of the flow and

$$U_s = \frac{k_{1\alpha}[\mathrm{MA}][\mathrm{I_2}]}{k_2[\mathrm{ClO_2}](k_{1\beta} + [\mathrm{I_2}])}, \quad V_s = \frac{(k_{1\alpha}[\mathrm{MA}])^2[\mathrm{I_2}]}{k_{3\beta}k_2[\mathrm{ClO_2}](k_{1\beta} + [\mathrm{I_2}])^2}. \tag{12}$$

This leads to the equations, on dropping the bars for convenience,

$$\frac{\partial c_1}{\partial t} + \mathbf{v}(\mathbf{r},t)\cdot\nabla c_1 = \mathrm{Da}\left(1 - c_1 - \frac{4c_1c_2}{\beta + c_1^2}\right) + \mathrm{Pe}^{-1}D\nabla^2 c_1, \tag{13}$$

$$\frac{\partial c_2}{\partial t} + \mathbf{v}(\mathbf{r},t)\cdot\nabla c_2 = \mathrm{Da}\alpha\left(c_1 - \frac{c_1 c_2}{\beta + c_1^2}\right) + \mathrm{Pe}^{-1}\nabla^2 c_2, \tag{14}$$

where

$$\mathrm{Da} \equiv \frac{k_2[\mathrm{ClO}_2]L}{U_0}, \quad \mathrm{Pe} \equiv \frac{LU_0}{D_{c_2}}, \quad D \equiv \frac{D_{c_1}}{D_{c_2}} \tag{15}$$

are the Damköhler and Péclet numbers and D is the ratio of the diffusion coefficients corresponding to the two different components. $k_2[\mathrm{ClO}_2]$ is the reference reaction rate. We note that the Damköhler number measures the ratio of the chemical and advective time scales and the Péclet number gives the ratio between the advective and diffusive transport. Large Damköhler numbers correspond to slow stirring or equivalently fast chemical reaction and vice versa. Péclet numbers are usually large, which is the case considered here, therefore diffusion alone is not efficient in removing concentration gradients at large scales. In the present study a range of values of the Damköhler number are explored with the Péclet number fixed at a large value. α and β are two chemical (kinetic) parameters given by

$$\alpha = \frac{U_s}{V_s}, \quad \beta = \frac{k_{3\gamma}}{U_s^2}. \tag{16}$$

The dimensionless scalings of the kinetics in Eqs. (13) and (14) are a modified version of those used originally by Epstein and Lengyel [13,14], and are the same as those used previously in Refs. [27,28]. In particular, the explicit appearance of the parameter β in these scalings allows the nature of the Hopf bifurcation to be more clearly identified. The kinetic scheme, essentially dimensionless versions of Eqs. (9) and (10), has a steady state $(c_1^s, c_2^s) = \left(\frac{1}{5}, \frac{1}{25} + \beta\right)$ which is stable for $\alpha > \alpha_H = \frac{3}{5} - 25\beta$. This loses stability at $\alpha = \alpha_H$ through a Hopf bifurcation. For $\beta > \beta_0 \simeq 2.9 \times 10^{-3}$, this bifurcation is supercritical, producing stable limit cycles if $\alpha < \alpha_H$. For $\beta < \beta_0$ the bifurcation is subcritical, giving a range of $\alpha > \alpha_H$ at which there exists both a stable steady state and a stable limit cycle. We consider these two scenarios in our numerical simulations.

III. NUMERICAL SIMULATIONS

We integrated the advection-diffusion-reaction problem (13) and (14) on a square $\Omega = [0,1] \times [0,1]$, using 1000×1000 grid points, applying periodic boundary conditions. The numerical method used a semi-Lagrangian scheme for the advection combined with an explicit scheme for diffusion and a fourth-order Runge-Kutta method for the time integration of the local dynamics. The advection step used a semi-Lagrangian scheme at time t_0 which consists of computing, at each grid point, a backward-time Lagrangian trajectory for a time Δt. The concentrations at this fluid element are calculated by bilinear interpolation using values of the concentrations at time $t_0 - \Delta t$ and these values are assigned to the original lattice point at time t_0. The values of the Péclet number and D were kept constant, $\mathrm{Pe} = 10^4$, $D = 1.0$. The time step used was $\Delta t = 0.001$ and the period of the flow was set at $T_f = 1.0$.

A check on the accuracy of the numerical scheme can be provided by the $\mathrm{Da} = 0$ case, where the total concentrations of c_1 and c_2 should remain constant throughout as reaction effects are removed. The mean values of c_1 and c_2 were calculated from the numerical results in the $\mathrm{Da} = 0$ case and were found to remain constant to at least ten decimal places. This gives confidence that our results for $\mathrm{Da} \neq 0$ are also reliable.

A. Supercritical case, $\beta > \beta_0$

We start by considering the case when the Hopf bifurcation in the kinetic equations is supercritical, i.e., $\beta > \beta_0$. Here we can only have either a stable steady state (if $\alpha > \alpha_H$) or a stable limit cycle (if $\alpha < \alpha_H$). Thus only values of $\alpha < \alpha_H$ are relevant for this section and we took $\alpha = 0.375$ and $\beta = 0.005$ for these computations. The evolution of an initial perturbation is investigated for different values of the Damköhler number, comparing the cases of zero (unreactive) and nonzero (reactive) Damköhler numbers.

Initially the system is homogeneous in space ($c_1 = \frac{1}{2}c_1^0$, $c_2 = \frac{1}{2}c_2^0$ at $t = 0$ for all $\mathbf{r}$ in Ω). If $(c_1^0, c_2^0) \neq (c_1^s, c_2^s)$ the whole system oscillates homogeneously and there are no phase differences or fluctuations. The transport processes in this situation have no influence as there are no concentration gradients and the whole system is governed only by the nonlinear chemical dynamics. Different points in the domain can be regarded as independent nonlinear oscillators. At this stage a perturbation in the form

$$c_1(x,y,0) = \frac{1}{2}c_1^0(1 + \{1 + 2\delta \sin[2\pi(x-y)]\}),$$

$$c_2(x,y,0) = \frac{1}{2}c_2^0(1 + \{1 + 2\delta \sin[2\pi(x-y)]\}) \tag{17}$$

is applied, where δ is the amplitude of the perturbation. We take $\delta = 0.5$ in the numerical simulations. From the spatial distributions (a typical example is shown in Fig. 1 for $\mathrm{Da} = 0.65$) it can be observed that the initial perturbation given by Eq. (17) (Fig. 1, first plot) is folded and stretched by the chaotic advection into increasingly thinner filaments, see Fig. 1 (second to fourth plots). These filaments grow in length and gradually invade the whole domain with a decrease in the local amplitude of the inhomogeneity. At this stage the filaments overlap and all the points in the domain fluctuate around some mean, see Fig. 1 (fifth to seventh plots). In this phase the characteristic pattern of the spatial structure (unstable manifold of the advection dynamics) is not changing apart from the relatively fast decay of the overall amplitude of the fluctuations. The final state is complete homogenization with the system oscillating in phase, see Fig. 1 (eighth and ninth plots).

For the case $\mathrm{Da} = 0$ (unreactive system) it has been shown previously [4–6], that an initial impurity (passive scalar field) is homogenized by the joint action of advection and diffusion. Chaotic advection acts very efficiently on large

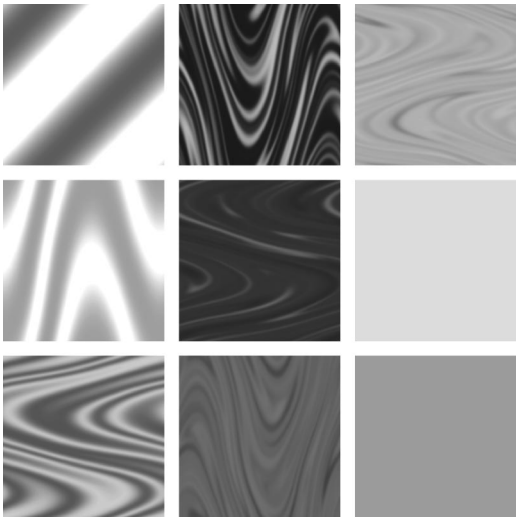

FIG. 1. gray level plots of the time evolution of c_1 for Da $=0.65$ obtained from the numerical integration of Eqs. (13) and (14). Plots 1–7 are at equal time intervals ($\Delta t=0.5$) from $t=0$ to $t=3.0$, plots 8 and 9 are at $t=17.0$ and $t=19.5$ ($\alpha=0.375$, $\beta=0.005$, Pe$=10^4$, $D=1.0$). The time evolution of the consecutive plots is from top to bottom and from left to right.

scales creating sharp concentration gradients for a more efficient diffusive transport at small scales. In these studies it has been shown that the different moments of the deviation of the local concentration form the mean concentration decay exponentially in time [4–6]. Thus, for example, the standard deviation of the concentration field evolves in time as

$$\sigma_c(t) = \sqrt{\langle c^2(t,x,y)\rangle - \langle c(t,x,y)\rangle^2} \sim \exp(-\lambda t), \qquad (18)$$

where $\langle\ \rangle$ represents averaging over the whole domain. A plot of the standard deviation in the c_1 concentration field, σ_{c_1}, against time for our system is shown in Fig. 2 on a lin-log plot. We note that σ_{c_2} has the same behavior as σ_{c_1}, so for simplicity only σ_{c_1} needs to be considered. In Fig. 2 we plot σ_{c_1} for the unreactive case (Da$=0$) by the smooth line and show σ_{c_1} for cases when Da$\neq 0$ by oscillatory lines.

Consider the unreactive case first. In the early stages the standard deviation stays almost constant due to the fact that the loss in the amplitude of the perturbation is compensated by the exponential growth in length of the filaments. Diffusion is almost negligible in the beginning as there are only large scale structures in the concentration distribution. After the filaments have invaded the whole domain they start overlapping and interacting and small scale structures are formed making diffusion more efficient. This leads to an exponential decay of the standard deviation with $\lambda \simeq 0.7867$. The inverse of the decay rate of the standard deviation λ^{-1} defines a characteristic time scale associated with the decay of an initial perturbation due to the combined effects of advection and diffusion.

We now consider the effect that a nonzero Damköhler number has on the overall dynamics. By measuring the period and the Floquet exponent of the limit cycle Γ of the (dimensionless) kinetic scheme, we can define a decay rate

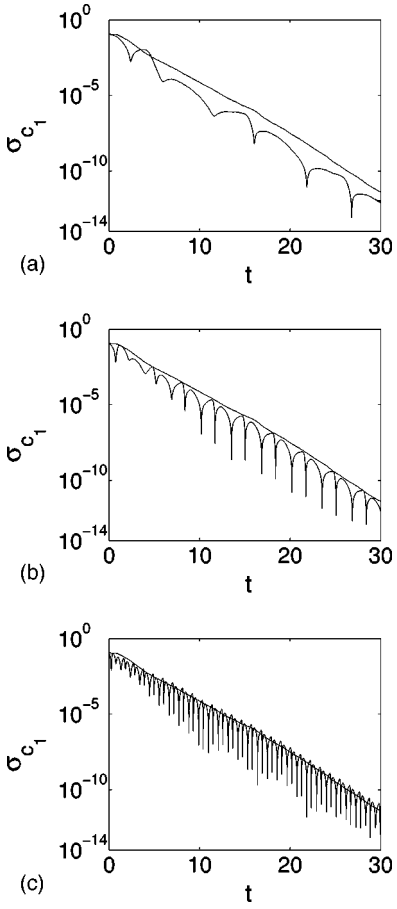

FIG. 2. The standard deviation σ_{c_1}, defined in Eq. (18), obtained from the numerical integration of Eqs. (13) and (14), plotted against t for (a) Da$=0.2$, (b) Da$=0.65$, (c) Da$=2.0$ (shown by the oscillatory lines). The result for the unreactive case (Da$=0$) is shown by the smooth line ($\alpha=0.375$, $\beta=0.005$, Pe$=10^4$, $D=1.0$).

corresponding to the stable limit cycle, as $\mu=|\rho_\gamma/T_c(\mathrm{Da})|$, where ρ_γ is the Floquet exponent corresponding to the limit cycle and is independent of the Damköhler number. A direct consequence of Da multiplying the chemical dynamics in Eqs. (13) and (14), is the dependence of T_c on Da according to $T_c(\mathrm{Da})=T_c(\mathrm{Da}=1)/\mathrm{Da}$. μ shows how fast a point in the phase space is attracted to the limit cycle. Thus μ^{-1} defines a characteristic time scale of the chemical dynamics. For Da $=1$ and the other parameters used in the numerical simulations $T_c=2.172$ and the corresponding Floquet exponent is $\rho_\gamma=-2.603$. This gives a chemical time scale of $\mu=2.603\mathrm{Da}/T_c$ (Da$=1$). Hence a value of Da$=0.65$ gives comparable characteristic decay rates for the chemical kinetics and mixing. We consider this value of Da as well as Da $=0.2$ and Da$=2.0$ which give, respectively, decay rates for the chemical reaction that are approximately three times slower and three times faster than the decay rate in the purely advection-diffusion case.

In Fig. 2 we plot the standard deviation of the spatial distribution of the first component, σ_{c_1}, for Da $=0.2, 0.65, 2.0$ as a function of time on a lin-log plot. The oscillations in the standard deviation are due to the oscillating nonlinear chemical dynamics. As mentioned above the

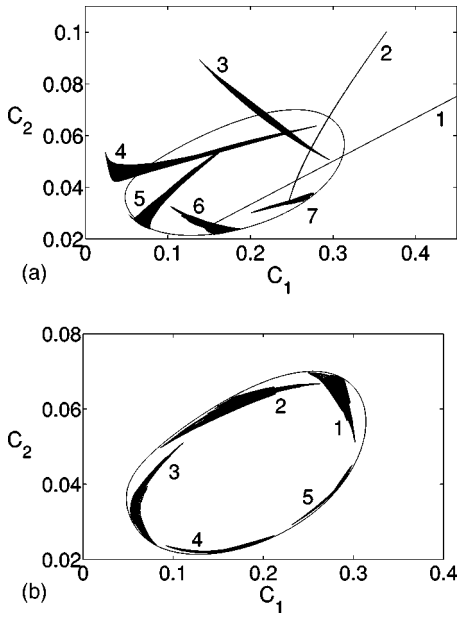

FIG. 3. Plots of the development of the initial perturbation (17) in the (c_1, c_2) phase plane for (a) Da=0.65 with $\Delta t=0.5$ from $t=0$, (b) Da=2.0 with $\Delta t=0.2$ from $t=2.4$ ($\alpha=0.375$, $\beta=0.005$, Pe$=10^4$, $D=1.0$).

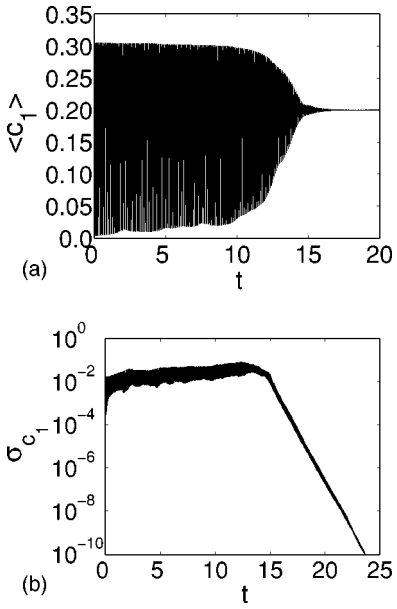

FIG. 4. (a) $\langle c_1 \rangle$, the average value of c_1 defined by Eq. (19) and (b) the standard deviation σ_{c_1}, defined by Eq. (18), plotted against t obtained from a numerical integration of Eqs. (13) and (14), for Da=22.0 and $\Delta=0.05$ (radius of the initial perturbation) ($\alpha=0.62$, $\beta=0.0001$, $D=1$, Pe$=10^4$, $dt=0.001$).

increase of the frequency with Da is explained by the dependence of T_c on Da. Comparing the unreactive case with the reactive cases in Fig. 2, shows that the change of Da has no significant effect on the decay rate of the standard deviation σ_{c_1}. The decay rates for Da=0.65 ($\lambda \simeq 0.7827$) and for the unreactive case are directly comparable. However, there is an indication that the homogenization process is slightly faster for Da=0.2 ($\lambda \simeq 0.8223$) and slightly slower for Da=2.0 ($\lambda \simeq 0.7731$) than for the unreactive case, though these tendencies are only marginal at best. This trend of a slightly slower decay of the standard deviation for larger Damköhler numbers does not become more accentuated if the Damköhler number is further increased. Computations for Da=4.0 ($\lambda \simeq 0.7732$) and 6.0 ($\lambda \simeq 0.7725$) show that the decay rate of the standard deviation is essentially the same at that found for Da=2.0.

We can use our results to plot phase plane diagrams, i.e., plots of c_2 against c_1 obtained from our numerical data at a given time. Plots for Da=0.65 and Da=2.0 are shown in Fig. 3, plotted at equally spaced time intervals ($\Delta t=0.5$ for Da =0.65 and $\Delta t=0.2$ for Da=2.0). The limit cycle in the kinetic system is shown by the closed loop. These diagrams provide an explanation as to why the chemical reaction has little overall effect on the homogenization process. When the mixing is much faster than the chemical kinetics (small Da), homogenization of the concentrations happens before the limit cycle is reached. When there is slow mixing (large Da), points in the phase space are quickly attracted to the limit cycle and, as the chemical dynamics is neutrally stable with respect to perturbations along the limit cycle, the concentration fluctuations are dissipated only by mixing and diffusion. In both cases the homogenization rate is dominated by the coupled effect of mixing and diffusion, therefore is largely independent of the reaction rate measured through Da. We note that the concentrations of c_1 and c_2 outside the limit cycle are much more rapidly attracted to it than those within. This can be explained by the time variation along the limit cycle, which is described slowly for the parts where c_1 and c_2 have their higher values and quickly where their values are lower. Thus the higher concentrations of c_1 and c_2 have a much longer time periods when they are relatively close to the limit cycle and thus can be attracted to it.

B. Subcritical case, $\beta < \beta_0$

For $\beta < \beta_0$ there is a range of $\alpha > \alpha_H$ where a stable steady state and a stable limit cycle coexists in the kinetic scheme and it is this case that we now examine. We took $\alpha=0.62$, $\beta=0.0001$, $D=1$ and an initial perturbation in which a central region (of radius Δ) was set at the steady state (c_1^s, c_2^s) with the rest of the reactor uniform in space and oscillating in time. Both states are stable in the kinetic scheme for these parameter values [28]. For the smaller values of Da the initial state became homogenized within the oscillatory behavior in the same way as described above. However, for larger values of Da this is not the case. Now the effect of the relatively weak mixing within the chaotic advection and the relatively strong chemistry is to allow the steady state to spread through the reactor. Eventually this steady state dominates and the reactor is everywhere at its spatially homogeneous steady state (c_1^s, c_2^s).

We illustrate this behavior in Fig. 4, where we plot the average value $\langle c_1 \rangle$ of c_1, given by

$$\langle c_1 \rangle(t) = \iint c_1(x,y,t)\,dx\,dy \tag{19}$$

and the standard deviation σ_{c_1}, defined by Eq. (18), for Da =22.0 and $\Delta=0.05$. The figure shows that the system has a

relatively long period of oscillatory behavior for this value of Da, undergoing many oscillations until $t \simeq 10$ before there is a rapid change to the steady state by $t \simeq 15$. This suggests that both oscillatory and steady states can exist simultaneously for a relatively long time before there is a rapid transition to steady behavior everywhere. The decay of the standard deviation in Fig. 4(b) is much faster than in Fig. 2 due to the stronger attraction to the stable homogeneous steady state.

As the value of Da is decreased from Da=22.0 the length of time that the oscillating and steady states exist simultaneously increases before the steady state fills the whole region. This makes it difficult to determine the critical Damköhler number precisely for this transition from oscillatory to steady behavior at large times and suggests a "saddle-node type" bifurcation for this transition. Our numerical results indicate that the changeover from oscillations to steady states occurs between Da=21 and Da=22. As the Damköhler number is increased from Da=22.0 the length of time that the oscillations exist decreases with the steady state invading the system more rapidly.

It is worth mentioning that the critical Damköhler number depends on the extent of the area in the central region of the domain which is set to the steady state. A larger radius for this perturbation requires a smaller critical Damköhler number. In the alternative situation, where the whole reactor is in the steady state except in a localized central region which is oscillatory, it is also possible to obtain two different final states in the reactor, either the steady state or homogeneous oscillation. However, in this case, the size of the initial perturbation is much more important in determining the final outcome than in the previous setup.

The Lagrangian filament model, which reduces the 2D problem to a 1D analog has proved useful in giving insights into some of the transitions seen in 2D advection-reaction-diffusion systems and this 1D model is described in the next section for our specific problem.

IV. LAGRANGIAN FILAMENT MODEL

The repeated stretching and folding of fluid elements in the chaotic advection causes an initial spatial perturbation to evolve into complex spatial structure which eventually fills the whole domain. In the initial stage, however, a clear background exists and the filaments are well-defined. The chaotic nature of the 2D flow ensures the existence of a negative and positive Lyapunov exponent $(-\lambda, +\lambda)$, corresponding to the advection dynamics $\dot{\mathbf{r}}=\mathbf{v}(\mathbf{r},t)$. Therefore, at any point in the flow, a convergent and a divergent direction can be associated to the eigenvectors $\pm\lambda$. Hence in a Lagrangian reference frame a fluid particle is subjected to a stagnation-type flow corresponding to the simplified advection dynamics, $v_x=-\lambda x$, $v_y=\lambda y$. Along the y axis (divergent direction) there is a continuous stretching of the initial perturbation, advective transport will dominate being much faster than diffusion. However, along the x axis (convergent direction) the formation of small scale structures indicates that advection, diffusion, and reaction need to be considered together. This leads to the one-dimensional (dimensionless) equations for the average profile across the filament in the convergent direction,

$$\frac{\partial c_1}{\partial t} - x\frac{\partial c_1}{\partial x} = D\frac{\partial^2 c_1}{\partial x^2} + \tilde{\mathrm{Da}}\left(1 - c_1 - \frac{4c_1c_2}{\beta + c_1^2}\right),$$

$$\frac{\partial c_2}{\partial t} - x\frac{\partial c_2}{\partial x} = \frac{\partial^2 c_2}{\partial x^2} + \tilde{\mathrm{Da}}\alpha\left(c_1 - \frac{c_1c_2}{\beta + c_1^2}\right). \qquad (20)$$

Equations (20) represent the evolution of a transverse slice of a filament in a Lagrangian reference frame, the second term on the left-hand side is the mean convergent flow. The parameters are given by Eqs. (15) and (16), except that now the Damköhler number is $\tilde{\mathrm{Da}}=k_2[\mathrm{ClO}_2]/\lambda$. In this simplified model the folding effects of the 2D chaotic advection are completely lost, hence this model loses its validity when filaments start interacting (second stage in the homogenization process). A mean strain is assumed through λ, although in the 2D flow the strength of the stretching fluctuates in time and space. Equations (20) are defined on $-\infty < x < \infty$, $t>0$ with the zero-flux boundary conditions

$$\frac{\partial c_i}{\partial x} \to 0 \quad \text{as } |x| \to \infty \quad (i=1,2). \qquad (21)$$

We start by considering a linear stability analysis of Eq. (20) in two cases, one when c_1 and c_2 are oscillating uniformly in space, i.e., $c_1, c_2 \in \Gamma$ for all x and the other when the system is at its steady state $c_1=c_1^s$, $c_2=c_2^s$. For simplicity we restrict attention to the case $D=1$.

A. Linear stability analysis of the spatially homogeneous oscillations

We first consider small perturbations in the Lagrangian filament model (20) when c_1 and c_2 are oscillating everywhere in phase on the limit cycle Γ. Here it is more convenient to rescale time by $\bar{t}=\mathrm{Da}t$ and put

$$c_1(x,\bar{t}) = c_1^\gamma(\bar{t}) + C_1(x,\bar{t}), \quad c_2(x,\bar{t}) = c_2^\gamma(\bar{t}) + C_2(x,\bar{t}), \quad |C_1, C_2| \ll 1, \qquad (22)$$

where c_1^γ, c_2^γ are periodic functions of $\bar{t}$ with period T_c, independent of $\tilde{\mathrm{Da}}$. The (linear) equations for C_1, C_2 are, from Eq. (20),

$$\frac{\partial C_1}{\partial \bar{t}} = \frac{1}{\tilde{\mathrm{Da}}}\left(\frac{\partial^2 C_1}{\partial x^2} + x\frac{\partial C_1}{\partial x}\right) + a_\gamma(\bar{t})C_1 + b_\gamma(\bar{t})C_2,$$

$$\frac{\partial C_2}{\partial \bar{t}} = \frac{1}{\tilde{\mathrm{Da}}}\left(\frac{\partial^2 C_2}{\partial x^2} + x\frac{\partial C_2}{\partial x}\right) + c_\gamma(\bar{t})C_1 + d_\gamma(\bar{t})C_2, \qquad (23)$$

where a_γ, b_γ, c_γ, and d_γ are the elements of the Jacobian of the kinetics evaluated on $c_1^\gamma(\bar{t}), c_2^\gamma(\bar{t})$ and are periodic functions with period T_c.

We now use the basis functions to be defined in Sec. IV B in Eqs. (31) and (32), to construct a solution of Eqs. (23) in the form

$$(C_1, C_2) = \sum_{k=0}^{\infty} (u_k(\overline{t}), v_k(\overline{t})) W_k(x). \tag{24}$$

Substituting Eq. (24) into Eqs. (23) gives

$$\frac{d\mathbf{u}_k}{d\overline{t}} = [\mathbf{P}_\gamma(\overline{t}) - \tilde{\mathrm{Da}}^{-1}(2k+1)\mathbf{I}]\mathbf{u}_k \quad (k = 0, 1, 2, \ldots), \tag{25}$$

where

$$\mathbf{P} = \begin{pmatrix} a_\gamma & b_\gamma \\ c_\gamma & d_\gamma \end{pmatrix}, \quad \mathbf{u}_k = (u_k, v_k)^T,$$

and $\mathbf{I}$ is the unit matrix. If we put $\mathbf{u}_k = \exp[-(2k+1)\tilde{\mathrm{Da}}^{-1}\overline{t}]\mathbf{u}$ in Eq. (25) we obtain

$$\frac{d\mathbf{u}}{d\overline{t}} = \mathbf{P}_\gamma \mathbf{u} \tag{26}$$

and it is Eq. (26) that determines the Floquet exponents for the limit cycle Γ. Note that the translational invariance of the limit cycle solutions $c_1^\gamma(\overline{t}), c_2^\gamma(\overline{t})$ means that one (of the two) Floquet exponents is zero. Now Eq. (26) has a solution such that $\mathbf{u}(\overline{t}+T_c) = e^{\rho_\gamma T_c}\mathbf{u}(\overline{t})$ for all $\overline{t}$ for the other Floquet exponent ρ_γ [30]. Hence Eq. (25) has a solution which has

$$\mathbf{u}_k(\overline{t}+T_c) = e^{[\rho_\gamma - (2k+1)\tilde{\mathrm{Da}}^{-1}]T_c}\mathbf{u}_k(\overline{t}) \quad \text{for all } \overline{t}. \tag{27}$$

If Γ is a stable limit cycle then $\rho_\gamma < 0$ and expression (27) shows that this limit cycle behavior is also stable in the Lagrangian filament model.

The above analysis shows that the spatially homogeneous limit cycle $(c_1^\gamma(t), c_2^\gamma(t))$ is stable to small perturbations for all $\tilde{\mathrm{Da}}$. This result is in line with the two-dimensional findings and explains the mechanism by which homogenization happens in the initial stages of the 2D case. If $\alpha > \alpha_H$ the same stability property is valid for the spatially homogeneous steady state (c_1^s, c_2^s) (see Sec. IV B). When $\beta < \beta_0$ the Hopf bifurcation is subcritical and it is possible to have both these states existing for the same value of α. This occurs, for example, when $\alpha = 0.62$, $\beta = 0.0001$, which is the case that we consider for our filament model. We started numerical simulations with the system oscillating homogeneously and then applied a perturbation which put a region around $x = 0$ to the steady state (c_1^s, c_2^s). We solved Eqs. (20) with $D = 1$ for increasing values of $\tilde{\mathrm{Da}}$ as well as varying the extent of the perturbation region. For the smaller values of $\tilde{\mathrm{Da}}$, up to $\tilde{\mathrm{Da}} \simeq 15.0$, the system returned to its spatially homogeneous oscillatory state, no matter how large we made the perturbed region. For $\tilde{\mathrm{Da}}$ greater than $\tilde{\mathrm{Da}} = 20.0$ we found, for a sufficiently large perturbed region, very weak oscillations about the steady state (close to $x = 0$) and spatially uniform oscillations (for larger x) existing simultaneously, with a relatively thin transition region between these two regimes. This behavior, illustrated in Fig. 5 for $\tilde{\mathrm{Da}} = 20.0$, persists for all the higher values of $\tilde{\mathrm{Da}}$ tried, with the size of the perturbed region needed to initiate it reducing in extent. If, in the two-dimensional subcritical case, the whole reactor is set to oscillate homogeneously in space except for a small central region which is set to the steady state, then filaments with their central region very close to steady state, as presented above in the filament model, can form and propagate eventually filling in the whole domain. Thus a transition of the system from oscillations to steady state can take place as presented in Fig. 4.

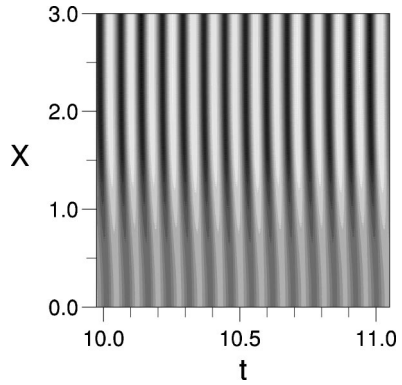

FIG. 5. A gray-level plot of c_1 obtained from the numerical integration of Eqs. (20) for $\tilde{\mathrm{Da}} = 20.0$ and $\alpha = 0.62$, $\beta = 0.0001$, $D = 1.0$.

We also tried the alternative procedure of starting the numerical simulations with the system in its homogeneous steady state and perturbing around $x = 0$ to the stable limit cycle. In all these computations the system returned to the homogeneous steady state no matter how large a value of $\tilde{\mathrm{Da}}$ or perturbed region was tried. An explanation is suggested by the purely reaction-diffusion system [Eqs. (20) with the flow terms neglected]. Here the tendency is for the stable steady state to propagate into the oscillatory region. The effect of the flow is to counteract this tendency and gives the possibility of a balance between the outward propagation of the steady state and the inflow of the oscillatory behavior. If the situation is reversed, the flow reinforces the tendency of the homogeneous steady state to propagate out from its initial region.

B. Linear stability analysis of the steady state

For this second case we write

$$c_1(x,t) = c_1^s + C_1(x,t), \quad c_2(x,t) = c_2^s + C_2(x,t), \quad |C_1, C_2| \ll 1 \tag{28}$$

and obtain the linear equations

$$\frac{\partial C_1}{\partial t} = \frac{\partial^2 C_1}{\partial x^2} + x\frac{\partial C_1}{\partial x} + \tilde{\mathrm{Da}}\left(\frac{3 - 125\beta}{1 + 25\beta}C_1 - \frac{20}{1 + 25\beta}C_2\right),$$

$$\frac{\partial C_2}{\partial t} = \frac{\partial^2 C_2}{\partial x^2} + x\frac{\partial C_2}{\partial x} + \tilde{\mathrm{Da}}\left(\frac{2\alpha}{1 + 25\beta}C_1 - \frac{5\alpha}{1 + 25\beta}C_2\right). \tag{29}$$

We look for a solution of Eqs. (29) in the form

$$(C_1, C_2) = \sum_{k=0}^{\infty} (a_k, b_k) e^{\sigma_k t} W_k(x), \tag{30}$$

where the a_k, b_k are constants and where the basis functions $W_k(x)$ $(k=0,1,2,\ldots)$ satisfy

$$W_k'' + xW_k' + (2k+1)W_k = 0 \tag{31}$$

and are chosen so as to satisfy the symmetry condition $W_k'(0)=0$ and be exponentially small as $x \to \infty$. The solution to Eq. (31) can be expressed as

$$W_k(x) = e^{-x^2/2}\, {}_1F_1\left(-k; \frac{1}{2}; \frac{x^2}{2}\right) \quad (k = 0,1,2,\ldots), \tag{32}$$

where ${}_1F_1\left(-k; \frac{1}{2}; x^2/2\right)$ are confluent hypergeometric functions [29] and, with k a positive integer, are polynomials in x^2 of order x^{2k}.

Applying Eqs. (30) and (31), in Eqs. (29) gives the equation for σ_k as

$$\sigma_k^2 + \left[(4k+2) - \tilde{\mathrm{Da}}\left(\frac{3-5\alpha-125\beta}{1+25\beta}\right)\right]\sigma_k + (2k+1)^2 - \tilde{\mathrm{Da}}(2k+1)\left(\frac{3-5\alpha-125\beta}{1+25\beta}\right) + \frac{25\alpha}{(1+25\beta)}\tilde{\mathrm{Da}}^2 = 0. \tag{33}$$

If the steady state (c_1^s, c_2^s) is stable in the kinetic scheme, i.e., $\alpha > \alpha_H = 3/5 - 25\beta$, then Eq. (33) gives $\mathrm{Re}(\sigma_k) < 0$ for all k and this state is also stable in the Lagrangian filament model. If $\alpha < \alpha_H$ and the steady state is unstable in the kinetic scheme, Eq. (33) shows that there is the possibility of a Hopf bifurcation when $\tilde{\mathrm{Da}} = (4k+2)(1+25\beta)/(3-5\alpha-125\beta)$, giving a minimum value of $\tilde{\mathrm{Da}}$ for this instability at

$$\tilde{\mathrm{Da}}_H = \frac{2(1+25\beta)}{3-5\alpha-125\beta}. \tag{34}$$

For this bifurcation to occur the final (constant) terms in Eq. (33) must be positive. Applying Eq. (34) in these terms in Eq. (33) shows that we must have

$$\alpha_H > \alpha > \alpha_1, \quad \text{where } \alpha_1 = \frac{13 + 125\beta - 4\sqrt{10(1+25\beta)}}{5} \tag{35}$$

for a Hopf bifurcation. For values of $\tilde{\mathrm{Da}} > \tilde{\mathrm{Da}}_H$ (and $\alpha > \alpha_1$) the steady state c_1^s, c_2^s is unstable in the Lagrangian filament model.

Equation (33) also shows the possibility of a saddle-node bifurcation (real root changing sign) where

$$\tilde{\mathrm{Da}} = \frac{2k+1}{50\alpha}(3 - 5\alpha - 125\beta \pm \sqrt{25\alpha^2 - 10\alpha(13+125\beta) + (3-125\beta)^2}). \tag{36}$$

This requires $\alpha < \alpha_1$ where α_1 is defined in Eq. (35). Equation (34) and the lower root in Eq. (36) (with $k=0$) identify a critical value of $\tilde{\mathrm{Da}}$ for the steady state c_1^s, c_2^s to be unstable in the Lagrangian filament model. This is illustrated in Fig. 6, for $\beta = 0.005$ for which $\alpha_1 = 0.04172$.

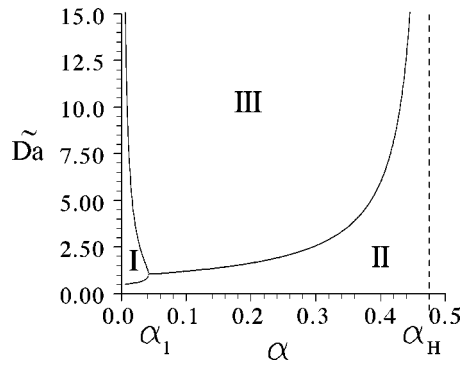

FIG. 6. Critical Damköhler numbers $\tilde{\mathrm{Da}}$ for the Lagrangian filament model given by Eqs. (34) and (36). In region II the steady state is stable and in region I and III the steady state becomes unstable.

We solved Eqs. (20) numerically with the system in its uniform steady state perturbed in a small region centered on $x=0$. We first considered the case when $\alpha < \alpha_1$, taking $\alpha = 0.02$, $\beta = 0.005$. For these parameter values, Eq. (36) gives $\tilde{\mathrm{Da}} = 0.5646$ for the system to become (linearly) unstable. Our numerical integrations showed a change from stable (region II in the bifurcation diagram plotted in Fig. 6), at $\tilde{\mathrm{Da}} = 0.5$ where the system returned to its spatially uniform steady state, to unstable (region I in the bifurcation diagram plotted in Fig. 6) at $\tilde{\mathrm{Da}} = 0.6$, consistent with this bifurcation value. For values just above the bifurcation value, up to $\tilde{\mathrm{Da}} = 0.9$, the numerical solutions approached a steady state with a spatially nonuniform profile associated with the first mode $(k=0)$ being unstable. This is illustrated in Fig. 7(a) with plots of the concentration c_1 for a range of values of $\tilde{\mathrm{Da}}$.

For higher values of $\tilde{\mathrm{Da}}$, spatially uniform oscillations, consistent with the limit cycles in the kinetic system, were quickly set up from the initial perturbation. However, there was a "window," from approximately $\tilde{\mathrm{Da}} = 6.0$ to $\tilde{\mathrm{Da}} = 7.0$, where more complex behavior was seen. In this range of $\tilde{\mathrm{Da}}$ the system was oscillatory for small values of x and steady for larger values, with a time dependent, spatially nonuniform profile joining the oscillatory region to the spatially uniform steady state at large x. This behavior is shown in Fig. 7(b) by a gray-level plot of c_1 for $\tilde{\mathrm{Da}} = 6.0$.

We next considered a value for α in the range $\alpha_1 < \alpha < \alpha_H$, taking $\alpha = 0.375$, again with $\beta = 0.005$, for which Eq. (34) gives $\tilde{\mathrm{Da}}_H = 4.5$. Our numerical computations showed that, for values of $\tilde{\mathrm{Da}}$ less than the bifurcation value (region II in the bifurcation diagram plotted in Fig. 6), the system returned to its spatially uniform steady state and, for values somewhat greater than $\tilde{\mathrm{Da}}_H$ (region III in the bifurcation diagram plotted in Fig. 6), spatially uniform oscillations were set up. For values of $\tilde{\mathrm{Da}}$ just above the bifurcation value, from approximately $\tilde{\mathrm{Da}} = 5.0$ to 8.5, more complex behavior arose, with the solution being oscillatory for small

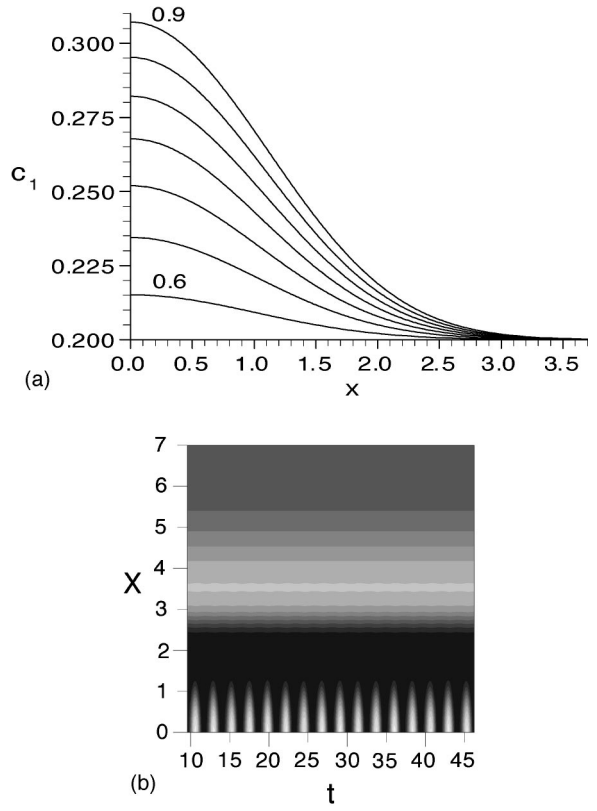

FIG. 7. (a) Steady profiles of c_1 obtained from the numerical integration of Eqs. (20) for $\alpha=0.02$, $\beta=0.005$, $D=1.0$ and for a range of values of $\tilde{\mathrm{D}}\mathrm{a}$ from 0.6 to 0.9. (b) A gray-level plot of c_1 for $\tilde{\mathrm{D}}\mathrm{a}=6.0$ and $\alpha=0.02$, $\beta=0.005$, $D=1.0$. The solutions of the Eqs. (20) presented above in (a) and (b) correspond to region I and III, respectively, in the bifurcation diagram plotted in Fig. 6.

values of x and at its steady state for higher values. This is illustrated in Fig. 8 with a gray-level plot of c_1 for $\tilde{\mathrm{D}}\mathrm{a}=7.0$.

V. CONCLUSIONS

We have considered the response of an oscillatory reaction stirred by a chaotic flow to different spatial perturbations. We considered the particular case of the CDIMA reaction, since this allowed us to treat two separate cases. One when uniform oscillation is the only stable state and the other when both oscillatory and steady behavior are stable states. In the first (supercritical) case, the initial perturbation is always homogenized and the system returns to spatially uniform oscillations. The decay rate of the spatial fluctuations is virtually the same as for a nonreactive component.

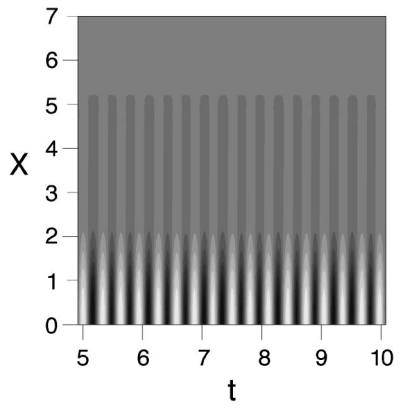

FIG. 8. A gray-level plot of c_1 obtained from the numerical integration of Eqs. (20) for $\tilde{\mathrm{D}}\mathrm{a}=7.0$ and $\alpha=0.375$, $\beta=0.005$, $D=1.0$. The solution of the Eqs. (20) presented above corresponds to region III in the bifurcation diagram plotted in Fig. 6.

When the kinetic system can have either a stable steady state or stable oscillations (subcritical case), we find that the reactor can behave in two possible ways. For smaller Damköhler numbers the initial perturbation is homogenized within the oscillatory response in a way similar to the supercritical case. However, for larger Damköhler numbers this does not always happen and an initial perturbation, setting a certain region to the steady state, can spread throughout the reactor, leaving it finally everywhere at this steady state. The reason for this is suggested by the Lagrangian filament model. The initial effect of the chaotic flow is to form thin filaments, separate from each other, in which the concentrations of the reactants are at their steady states. This initial phase can be described reasonably well by the 1D model, which we have seen can either return to the oscillatory state (smaller Da) or set up steady states within the background oscillations (larger Da), see Fig. 5. Thus for the smaller values of Da the concentrations within the filaments become oscillatory and, as they are stretched further and interact spreading through the reactor, the uniform oscillatory response returns. However, for larger Da, the concentrations in the filaments remain at the steady state and the further stretching and folding caused by the chaotic flow spreads this steady state throughout the reactor, leading to the relatively rapid collapse of the oscillations seen in Fig. 4.

Many experimental studies (see Ref. [10] for a detailed list of references) have investigated the effects of stirring on nonlinear chemical dynamics, especially in the continuously stirred tank reactor (CSTR) configuration, and have shown that a spatially distributed system may behave qualitatively and quantitatively differently from its homogeneous reference system. The heterogeneity due to imperfect mixing, coupled with the nonlinear dynamics, can give rise to a much richer behavior of the system, i.e., oscillations, quenching of oscillations and even chaotic oscillations. For bi-stable systems it has been shown that the final state of the system can be changed by varying the stirring rate and our results for $\beta=0.0001$ have confirmed that, by changing the stirring rate through the Damköhler number, the system either settles to a uniform steady state or oscillates homogeneously at sufficiently long times.

The present problem can be thought of as a model for a reactor operating in batch mode, with the chaotic flow representing imperfect mixing within the reactor. In this situation we would expect the final state to be spatially homogeneous (oscillatory or steady). An alternative type of reactor that is often used is the flow reactor (CSTR) in which there is a continuous inflow of fresh reactants with the products of reaction continuously leaving the reactor. For a perfectly mixed reactor, the dynamics of the CDIMA reaction are modified by the flow rate [28] with now two values of α at which a Hopf bifurcation can occur and a critical flow rate above which the reactor is stable for all α.

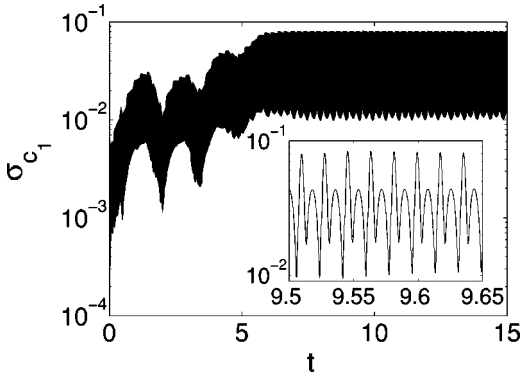

FIG. 9. The standard deviation σ_{c_1}, defined by Eq. (18), plotted against t obtained from the numerical integration of Eqs. (13) and (14), by replacing the sinusoidal shear flow with the open blinking vortex-sink system for Da=85 (α=0.62, β=0.0001, D=1, Pe=10^4, dt=0.001).

A model for imperfect mixing for this type of reactor could be provided by a chaotic flow with both an inflow and an outflow, the "blinking vortex sink" for example [31,32]. This system has been shown capable of sustaining complex (temporally oscillating) structures in the combustion context [19,20] and so we might also expect complex structures in the present case. The ability of the 1D Lagrangian filament model to have regions of both steady and oscillatory behavior co-existing for the CDIMA reaction suggests that this sort of configuration might be maintained in this type of flow reactor.

To investigate the possibility of the co-existence of steady and oscillatory states in the 2D problem, we considered the case of an open flow modelled by the blinking vortex-sink system [31,32]. This open flow models the outflow from a large reservoir through two vortex-sinks which are some distance apart from each other and are opened and closed alternately. This flow has a characteristic period T_f and after every half period the active vortex sink switches position. The problem was solved on a square domain $\Omega=[0,L]\times[0,L]$ by applying zero-flux boundary conditions, thus allowing the whole domain to oscillate homogeneously if no spatial variation is imposed. The parameters of the flow are the same as those used in Ref. [19]. We considered two cases for the chemical dynamics, suggested by our stability analysis of the 1D model. In the first case we followed the development of an initial localized spatial region set to the steady state within background oscillations. The evolution of such a perturbation has already been investigated in the 1D filament model in the previous section. There we found that, for a sufficiently large value of $\widetilde{\mathrm{Da}}$, filaments consisting of very weak oscillations around the steady state in a central region surrounded by spatially uniform oscillations. For smaller values of $\widetilde{\mathrm{Da}}$ the spatially homogeneous oscillatory solution was restored.

This 2D open flow system provides the possibility for such filaments to form and propagate, so some similarity between the 1D and 2D cases could be expected. In Eqs. (13) and (14), we replaced the sinusoidal shear flow with the blinking vortex-sink flow and used the same numerical technique to integrate the revised equations. Two regimes have been found in the 2D problem as the Damköhler number was varied. If $\widetilde{\mathrm{Da}}$ is small (slow reaction/fast flow) the initial patch of steady state is elongated into thin filaments and starts leaving the domain through either of the vortex sinks. Due to the rapid outflow relative to the reaction rate the steady state cannot respond to this loss by converting sufficient oscillating fluid elements into steady and eventually the whole domain returns to spatially homogeneous oscillations. In the large Da regime (Da=85 or larger) (fast reaction/slow flow), the initial perturbation propagates much more rapidly, being able to balance the loss due to the outflow, and after a transient time a periodic response in the system is set up in which there are regions of both steady and oscillatory behavior. This is illustrated in the plot of the standard deviation σ_{c_1} of the c_1 concentration field in Fig. 9. As a consequence of the Damköhler number multiplying the chemical dynamics the period of the oscillations decreases with the factor Da

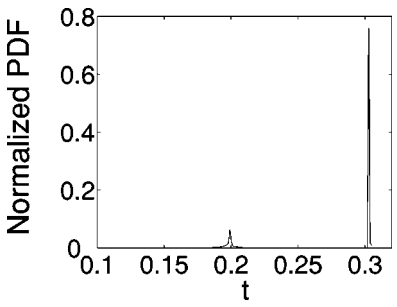

FIG. 10. Probability density function (pdf) of the concentration field c_1 sampled at time t=15 for Da=85 after the balance between steady and oscillatory states has been reached (α=0.62, β=0.0001, D=1, Pe=10^4, dt=0.001).

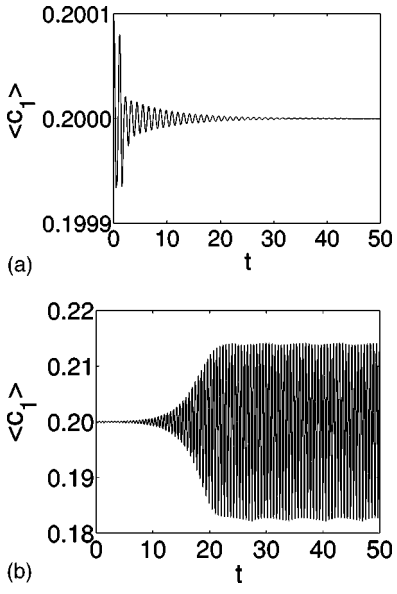

FIG. 11. Plots of the average concentration of c_1, defined by Eq. (19), against t for the open blinking vortex-sink system starting at the (unstable) steady state perturbed by local oscillations for (a) Da=2.0 and (b) Da=4.0 (α=0.375, β=0.005, D=1, Pe=10^4, dt=0.001).

which explains the very dense nature of the plot. In the inset a zoom in is given on a small time interval to show the periodic, period 2, response in the variance. By "binning" the c_1 values from the whole domain sampled at any time instant after the transients had died away and plotting the corresponding probability density function (pdf), two clear peaks can be seen (Fig. 10 at $t=15.0$). The high peak represents the background oscillation which is the most widespread in the domain and the smaller peak represents the steady state $c_1^s = 0.2$ confirming that the steady state and oscillations can co-exist in the 2D context as predicted by the 1D filament model.

The second scenario that we considered was the supercritical case, in which the system was at its spatially uniform (kinetically unstable) steady state with a small (central) region set to be oscillating. Our calculations for the 1D model, which includes flow effects, shows that the steady state is stable for smaller $\tilde{\mathrm{D}}\mathrm{a}$, becoming unstable (and oscillatory) at a critical value of $\tilde{\mathrm{D}}\mathrm{a}$, see Fig. 6 or expression (34). We find that this carries over into the 2D model, where we saw that, for smaller values of Da, the oscillations died out and the system returned to the uniform steady state everywhere. Even though this state is unstable in the kinetic scheme, the relatively fast mixing allows this state to be maintained in the reactor. A similar result is obtained in Ref. [17] for an autocatalytic reaction. For larger values of Da, the concentrations remain oscillatory within the filaments that develop in the flow. Thus, in this case, there are regions of both oscillatory (in the filaments) and steady (as background) responses. These two situations are illustrated in Fig. 11 with plots of $\langle c_1 \rangle$, the average concentration defined by Eq. (19), against t for $\mathrm{Da}=2.0$ [Fig. 11(a)] and $\mathrm{Da}=4.0$ [Fig. 11(b)], for both figures $\alpha=0.375$, $\beta=0.005$, $D=1.0$. Figure 11(a) shows the system returning to the steady state ($c_1^s=0.2$), whereas Fig. 11(b) shows a sustained oscillations about this steady state, again showing behavior predicted by the 1D model.

ACKNOWLEDGMENTS

We wish to acknowledge the support of the ESF Programme REACTOR and Istvan Zoltan Kiss wishes to thank ORS and the University of Leeds for financial support. We are grateful for useful discussion of this topic with Tamás Tél.

[1] H. Aref, J. Fluid Mech. **143**, 1 (1984).
[2] J. M. Ottino, *The Kinematics of Mixing: Stretching, Chaos and Transport* (Cambridge University Press, Cambridge, England, 1989).
[3] Z. Toroczkai, Gy. Karolyi, Á. Péntek, T. Tél, and C. Grebogi, Phys. Rev. Lett. **80**, 500 (1998).
[4] R. T. Pierrehumbert, Chaos, Solitons Fractals **4**, 1091 (1994).
[5] D. Rothstein, E. Henry, and J. P. Gollub, Nature (London) **401**, 770 (1999).
[6] D. R. Fereday, P. H. Haynes, A. Wonhas, and J. C. Vassilicos, Phys. Rev. E **65**, 035301(R) (2002).
[7] P. Rouff, Chem. Phys. Lett. **90**, 76 (1982).
[8] M. Menzinger and P. Jankowski, J. Phys. Chem. **90**, 1217 (1986).
[9] P. Sevcik and I. Adamcikova, Chem. Phys. Lett. **146**, 419 (1988).
[10] M. Menzinger and A. K. Dutt, J. Phys. Chem. **94**, 4510 (1990).
[11] P. De Kepper, J. Boissonade, and I. R. Epstein, J. Phys. Chem. **94**, 6525 (1990).
[12] I. Lengyel, J. Li, and I. R. Epstein, J. Phys. Chem. **96**, 7032 (1992).
[13] I. Lengyel and I. R. Epstein, Proc. Natl. Acad. Sci. U.S.A. **89**, 3977 (1992).
[14] I. Lengyel and I. R. Epstein, Acc. Chem. Res. **26**, 235 (1993).
[15] F. Városi, T. M. Antonsen, and E. Ott, Phys. Fluids A **3**, 1017 (1991).
[16] Z. Neufeld, Phys. Rev. Lett. **87**, 108301 (2001).
[17] Z. Neufeld, P. H. Haynes, and T. Tél, Chaos **12**, 426 (2002).
[18] Z. Neufeld, C. López, E. Hernández-Garcia, and O. Piro, Phys. Rev. E **66**, 066208 (2002).
[19] I. Z. Kiss, J. H. Merkin, and Z. Neufeld, Physica D **183**, 175 (2003).
[20] I. Z. Kiss, J. H. Merkin, S. K. Scott, P. L. Simon, S. Kalliadasis, and Z. Neufeld, Physica D **176**, 67 (2003).
[21] W. E. Ranz, AIChE J. **25**, 41 (1979).
[22] F. J. Muzzio and J. M. Ottino, Phys. Rev. Lett. **63**, 47 (1989).
[23] F. J. Muzzio and J. M. Ottino, Phys. Rev. A **40**, 7182 (1989).
[24] F. J. Muzzio and J. M. Ottino, Phys. Rev. A **42**, 5873 (1990).
[25] M. J. Clifford, S. M. Cox, and E. P.L. Roberts, Chem. Eng. J. **71**, 49 (1998).
[26] M. J. Clifford, S. M. Cox, and E. P . L. Roberts, Physica A **262**, 294 (1999).
[27] S. Kalliadasis, J. H. Merkin, and S. K. Scott, Phys. Chem. Chem. Phys. **2**, 2319 (2000).
[28] J. R. Bamforth, S. Kalliadasis, J. H. Merkin, and S. K. Scott, Phys. Chem. Chem. Phys. **2**, 4013 (2000).
[29] L. J. Slater, *Confluent Hypergeometric Functions* (Cambridge University Press, Cambridge, England, 1960).
[30] D. W. Jordan and P. Smith, *Nonlinear Ordinary Differential Equations* (Oxford University Press, Oxford, 1999).
[31] H. Aref, S. W. Jones, S. Mofina, and I. Zawadski, Physica D **37**, 423 (1989).
[32] Gy. Karolyi and T. Tél, Phys. Rep. **290**, 125 (1997).